Invited Paper

Experimental Demonstration of Laser Acceleration of Electrons via Relativistic Plasma Waves

C. E. Clayton, K. A. Marsh, A. Dyson, M. Everett, A. Lal, W. P. Leemans[a], R. Williams[b], and C. Joshi

Department of Electrical Engineering
University of California at Los Angeles
Los Angeles, CA 90024

[a] Present address: Lawrence Berkeley Laboratory, Berkeley, CA 94720
[b] Present address: Florida A & M University, Tallahassee, FL 32307

ABSTRACT

A two-frequency CO_2 laser beam was used to beat-excite a large amplitude electron plasma wave in a resonant density plasma. The accelerating fields of the relativistic plasma wave were probed with collinear injected 2.1 MeV electrons from an electron linac. Some electrons gained *at least* 7 MeV in traversing the approximately 1 cm length of the beat wave accelerator, with the measurement limited by the 9.1 MeV high energy cut-off of the detection system. The corresponding average acceleration gradient is > 0.7 GeV/m and the average wave amplitude n_1 / n_0 is > 8%. Estimates based on collective Thomson scattering indicate that peak wave amplitudes of 15–30% may have been achieved.

1. INTRODUCTION

Over the past ten years or so there has been a resurgence of interest in collective particle acceleration techniques using waves in plasmas because of their potential for the ultra-high gradient [O(GeV/m)] acceleration of particles[1]. These plasma waves can be resonantly excited as in the plasma beat wave acceleration scheme[2] or impulse-excited as wakes of either laser pulses as in the laser wakefield accelerator scheme[2,3] or of electron pulses as in the electron wakefield accelerator scheme[4]. The efficiency of the beat wave technique makes good use of current laser technology and has thus received most of the experimental attention. Experiments around the world have reported beat-excitation of relativistic electron plasma waves using lasers operating around 10 μm[5–7] and 1 μm[8,9]. However, no conclusive demonstration of controlled acceleration of externally injected electrons has been reported. If practical, such an accelerator could have impact on future high energy linear colliders, compact sources of tunable X-rays for materials and biological studies, and medical/industrial applications. In this experimental work, we demonstrate for the first time ultra-high gradient acceleration of externally injected electrons by laser-beatwave excited relativistic electron plasma waves.[10]

2. MODELING OF THE EXPERIMENT

2.1. Tunneling ionization

For our laser intensities, the time-dependent laser electric field $E(t)$ reaches a substantial fraction of the atomic electric field which has a characteristic magnitude $E_a = (m^2e^5)/\hbar^4 \approx 520$ GeV/m. In this case, the laser field can alter the shape of the binding potential of an electron in an atom as shown schematically in

 0-8194-1087-X/93/$6.00

Fig. 1(a). Essentially, the laser field lowers the potential barrier on one side of the atom thereby providing a finite probability that the electron will tunnel out of the potential well before the electric field changes sign. If ϕ_n is the ionization potential of the atom normalized to the ionization potential of hydrogen (13.6 eV), then the tunneling probability $W(t)$ is given by[11]

$$W(t) = \frac{4\pi e^2}{\hbar^3} \phi_n^{5/2} \xi \exp\left[-\frac{2}{3}\phi_n^{3/2}\xi\right] \tag{1}$$

where $\xi = E_a/E(t)$. The resulting plasma density $n(t)$ grows as

$$\frac{dn(t)}{dt} = W(t)[n_n - n(t)] \tag{2}$$

where n_n is the original neutral density. Figure 1(b) shows the calculated evolution of the plasma density using a model for our laser pulse which rises linearly to the peak intensity in 150 ps. Note that full ionization is reached in about 25 psec which is well before the peak of the pulse.

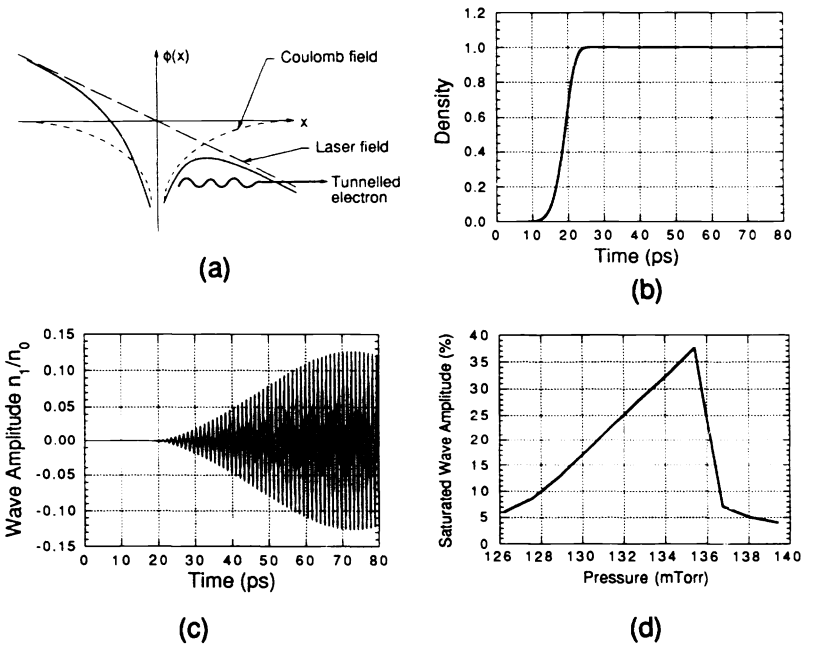

Figure 1: (a) Model for tunneling ionization of an atom. (b) Calculated rise of the plasma density relative to the neutral density. (c) Calculated growth of the plasma wave. (d) Calculated resonance of plasma wave with fill pressure. Resonant density is at 131.5 mT for full ionization.

2.2. Beat wave growth and saturation

Relativistic electron plasma waves are normal modes of the plasma with a phase velocity $v_\varphi \leq c$ such that the relativistic Lorentz factor associated with the phase velocity of the wave $\gamma_\varphi = \left[1-\left(v_\varphi/c\right)^2\right]^{-1/2}$ is much greater than unity. Two co-propagating laser beams with frequencies and wavenumbers (ω_1, k_1) and (ω_2, k_2) and intensities α_1 and α_2 interfere in space and time at $(\Delta\omega, \Delta k)$ and the beat-envelope of the interference, through the ponderomotive force, drives up a plasma wave of amplitude $\varepsilon = \Delta k \xi$ given by[12]

$$\frac{\partial}{\partial t}\left(\gamma\frac{\partial\xi}{\partial t}\right)+\omega_p^2\xi=\alpha_1\alpha_2\sin(\Delta\omega t-\Delta k\xi) \tag{3}$$

where $\Delta k=k_1-k_2$, $\Delta\omega=\omega_1-\omega_2$, ξ is the Lagrangian electron displacement variable describing the wave oscillating quantity, $\gamma=\left[1-(\dot{\xi}/c)^2\right]^{-1/2}$ is the Lorentz factor associated with the velocity of the electron oscillations in the wave, $\omega_p^2=4\pi n_o e^2/m$ is the square of the plasma frequency, n_o is the background plasma density, and the normalized electron quiver velocities are $\alpha_{1,2}=\frac{eE_{1,2}}{m\omega_{1,2}c}$ with the E_j being the laser electric fields. The electric field of the wave E_{accel} is related to its amplitude by $eE_{accel}=\varepsilon mc\omega_p$. The plasma responds to the driving force as a nonlinear harmonic oscillator. For plasma densities such that $\omega_p\approx\Delta\omega$ (the "resonant density" is the exact matching case but Eq. 3 predicts growth for a ± 3% band around resonant density), the wave will grow until the nonlinearity associated with γ leads to a "relativistic saturation". At this point, the frequency of the plasma wave has shifted (due to the relativistic mass change) enough that the driver and wave drift 180° out of phase whereupon the wave is driven down. The calculated growth of the plasma wave is shown in Fig. 1(c) for the case where the 3% lower than the resonant density. Here, $n_1/n_0=\varepsilon$ and is the wave amplitude expressed in terms of the modulation to the background density n_1 due to the wave. Figure 1(d) shows how the peak wave amplitude varies with density detuning. Note that tuning to a higher initial density helps to partly offset the relativistic mass increase, allowing the wave and driver to stay in phase longer and thus leading to larger wave amplitudes[13]. The optimum detuning for our pump strength requires a plasma density of 3% above resonance which in turn would yield a wave amplitude of about 37%.

2.3. Electron acceleration

For the experimental parameters summarized in Table 1, γ_φ (the Lorentz factor for the wave) is about 34. Imagining oneself in the wave frame, the background plasma electrons are streaming towards you (moving backwards in the wave frame) at nearly the speed of light and only slow down slightly as they rise over the crest of the potential hill of the wave. The work done on these background electrons by the wave is small because the electrons only spend a very short time in the accelerating phase of the wave. However, if one injects external electrons with sufficient initial velocity (or if the wave amplitude is large enough) then these injected electrons can be slowed down, stopped and reflected by the wave so that they are now moving forward in the wave frame. In this case, they can spend a relatively long time in the accelerating phase of the wave and thus gain a large amount of energy. For our expected wave amplitudes, we need to inject electrons with around 2 MeV of kinetic energy in order to be reflected or "trapped" by the wave.

The maximum longitudinal (accelerating) electric field E_L in the plasma wave is given by

$$E_L(\mathrm{GeV/cm})=\varepsilon\sqrt{n_o(\mathrm{cm}^{-3})} \tag{4}$$

which gives a range of fields of $0.5 < E_L$ (GeV/m) < 3.4 for our density and $0.05 < \varepsilon < 0.37$ which covers a range of amplitudes from the trapping threshold on the low side to the relativistic detuning limit on the high side. If, in the wave frame, the trapped electron can stay in the wave long enough to slide down the entire length of the potential hill (the so-called dephasing limit where the electron has out-run the wave) then it can gain the maximum kinetic energy given by $\Delta W_{max}=\varepsilon\gamma_\varphi^2 mc^2$. However, this requires a distance

L_{accel} in the lab frame of $L_{accel} \approx 2\gamma_\varphi^2 \lambda_p$ where $\lambda_p = 2\pi / \Delta k$ is the plasma wave wavelength. For our parameters, this length is about 30 cm which is much longer than the focal depth of our laser beam. Instead, we can calculate the maximum energy gain as simply $E_L L$ where L is some characteristic length of the experiment. For the 5–37% range of amplitudes and $L \approx 1$ cm, we should expect energy gains of 5 to 34 MeV. Since the injected electrons cover all phases of the plasma wave, the spectrum would have a continuous spectrum out to this maximum energy. The detailed shape of the spectrum depends strongly on the amplitude and length of the wave[14].

Table 1: Summary of the experimental parameters for the laser, plasma, and the electron linac.

Laser	Source	CO_2 laser
	Wavelengths	10.591, 10.289 μm
	Energy per line (typical)	60 J, 15 J
	Spot radius w_o	150 mm
	Rayleigh range $2z_o$	1.3 cm
	Electron quiver velocities	0.17, 0.07
	Pulse rise time	150 psec
	Pulse FWHM	300 psec
Plasma	Source	Tunnel ionization
	Density	8.6×10^{15} cm^{-3}
	Gas	Hydrogen
	Plasma period ν_p^{-1}	1.2 psec
	Plasma wave wavelength	360 μm
	Lorentz factor γ_{ph} for phase velocity	34
	Acceleration gradient for 10% wave	1 GeV/m
Electrons	Source	RF LINAC
	Energy	2.1 MeV
	Peak current	270 mA
	Emittance	6π mm-mrad
	Focused spot radius	125 μm
	RF frequency	9.3 GHz
	Micropulse separation	108 psec
	Electrons per micropulse	1.7×10^7
	Micropulse length (FWHM)	10 psec

Not all of the electrons from the electron injector can gain energy from the wave. The injected electrons have a range of radii and propagation angles as they enter the accelerating structure of the electron plasma wave. This spread in position and angle is characterized by the beam emittance ε_e. On the other hand, the plasma wave can accept electrons within a certain radius and within a certain angle (dependent on

the radial fields of the wave). This spread in position and angle that the plasma wave can capture (accelerate) is called the "acceptance" ε_a. It can be shown that the acceptance of the beat-excited plasma wave is approximately given by $\varepsilon_a = \sqrt{\frac{n_1}{n_0}\frac{1}{\gamma}\frac{2R}{9}}$ where R is the laser spot size and γ is the injected beam energy[15]. The capture efficiency η of the wave is then given by $\eta \approx c_L(\varepsilon_a/\varepsilon_e)^2$ where c_L is the longitudinal capture efficiency which is roughly 0.25 (only 1/4 of the wave is both focusing and accelerating). For our parameters, we expect $8\% < \eta < 30\%$ for $5\% < n_1/n_0 < 20\%$.

3. EXPERIMENTAL SETUP

3.1. The laser system and gas target

The CO_2 laser system[16] consists of an oscillator, a passive pulse shortening arrangement, and two stages of amplification. The hybrid oscillator produces a temporally smooth (single longitudinal mode) 100 nsec pulse. Two-frequency operation is obtained by the use of an intra-cavity absorption cell to balance the gain on the two lasing bands of interest (the 10P and 10R bands) and by adjusting the cavity length to select the two particular CO_2 lasing transitions. The two frequency pulse is shortened to about 100 psec via the plasma shutter and hot CO_2 cell through the optical free induction decay technique. After double-passing a low gain pre-amp and triple-passing a high pressure, high-gain power amplifier, the pulse has typically 60±10 J on the 10P(20) line at 10.591 μm and 10±5 J on the 10R(14) line at 10.289 μm. The pulse shape was measured by allowing the CO_2 light to gate a long, visible laser pulse in a Kerr cell. The gated green light was streaked and the data was linearized. The pulse has a rise time of about 150 psec and a 300 psec FWHM. The laser beam is focused with an f/11.5 off-axis parabolic mirror to a (measured) nearly diffraction-limited spot size of 300 μm diameter (for $1/e^2$ intensity fall-off) resulting in a peak intensity for the 10.6 μm beam of about 4.3×10^{14} W/cm^2 and normalized quiver velocities of $a_1 \approx 0.17$ and $a_2 \approx 0.07$. The vacuum chamber contains a static fill of around 140 mT of hydrogen gas. The plasma, produced by tunneling ionization of the gas[17], is imaged onto a CCD camera on every data shot. The images show plasma existing over more than 20 mm along the laser beam with a uniform core of about 10 mm in length. The full length at half the peak intensity of the focused beam (twice the Rayleigh length) was measured to be around 16 mm. According to Eq. 1, the laser has sufficient intensity to fully ionize the hydrogen at best focus by around 25 psec into the rising edge of the pulse and fully ionize over more than 12 mm on either side of best focus by the peak of the pulse.

3.2. The electron injector

The electric fields of the plasma wave are probed *directly* through the observed acceleration of injected electrons. The source of these electrons is an RF linac operating at 9.3 GHz[18] producing a train of about 10 psec FWHM pulses (the duration of these micropulses was measured by streaking optical Cherenkov radiation produced from a quartz test plate at the final focus) with 108 psec separation within a 2 nsec FWHM envelope (the macropulse). A schematic of the electron beamline and diagnostics is shown in Fig. 2(a). A sketch of the linac spot size along the beamline is shown in Fig. 2(b). There are three waists in the electron beam along the beamline. The first waist is at the 6 μm thick Mylar vacuum window. By focusing on the window, one minimizes the degradation to the beam emittance introduced by the window. The emittance after the window is 6π mm-mrad. The second waist is at the off-axis parabolic CO_2 focusing mirror. A small hole in the mirror allows us to introduce the electron beam along the CO_2 axis with minimal distortion of the laser beam. The final waist in the electron beam is at the interaction point of the experiment where the CO_2 beam is also focused. The spot size of the f/10-focused electrons is about 260 μm FWHM

which is comparable to the size of the CO_2 beam. The electron macropulse current is about 25 mA corresponding to about 1.7×10^7 electrons per 10 psec micropulse. The electrons have an energy of 2.1 MeV with a spread 5% FWHM. The laser and the electron *macro*pulse are electronically synchronized to ± 100 psec but the actual timing of the *micro*pulses is left to chance, as illustrated in Fig. 2(c). Clearly, we should expect a shot-to-shot success rate of about 30–50%. Note also that there are about 17 plasma wave periods within one micropulse so that the accelerated electrons will have some energy spread.

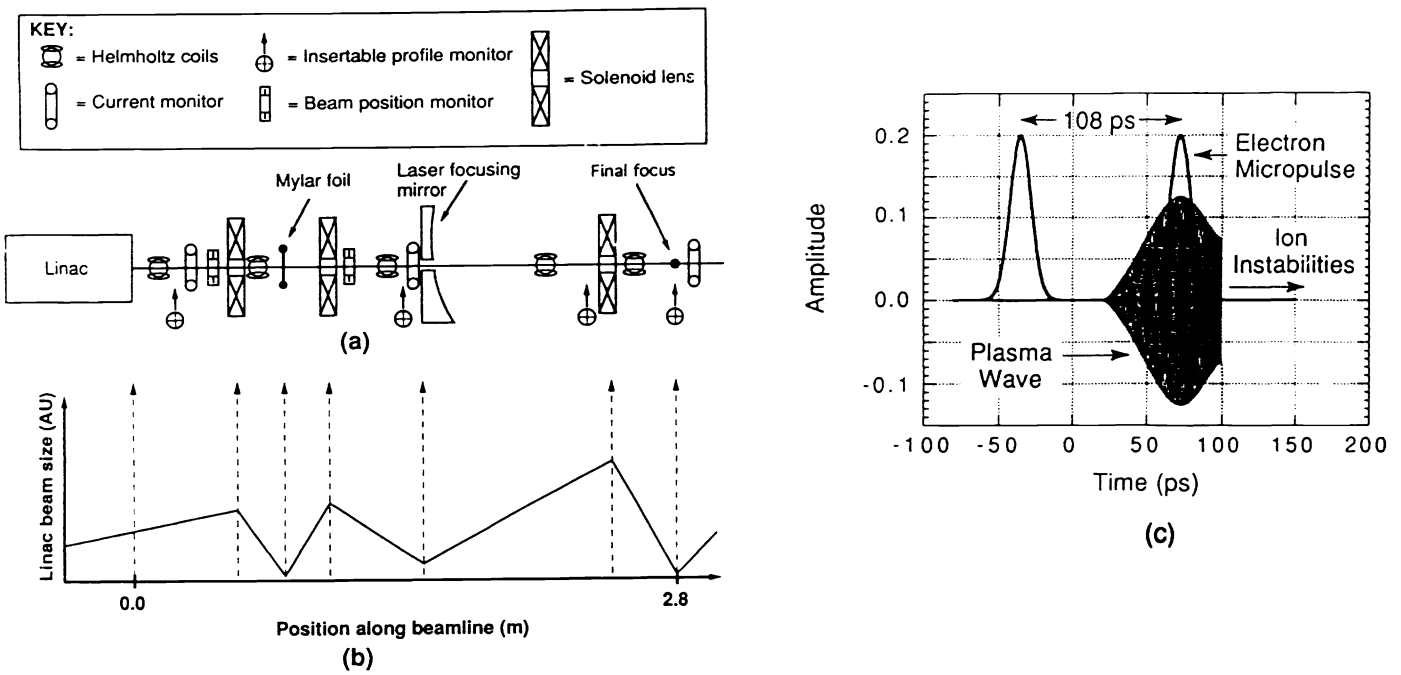

Figure 2: (a) Schematic of the electron beam line from the linac to the final focus at the interaction point and the various beam diagnostics. (b) Sketch of the electron beam spot size along the beam line. (c) A plot of the RF spacing of the electron micropulses and the calculated growth and saturation of the plasma wave.

3.3. Electron diagnostics

A detailed view of the experiment is shown in Fig. 3(a). The various electron trajectories are indicated on this figure. Both the accelerated and non-accelerated electrons enter a variable-field, imaging electron spectrometer[19]. The non-accelerated electrons are dumped onto low density plastic. Lead shielding reduces the flux of background X-rays reaching the electron detectors thereby reducing the background or noise levels to a value negligibly small compared to the signal levels ultimately obtained. The accelerated electrons exit the vacuum through a 25 μm thick Mylar window and are detected either electronically by one or more silicon surface barrier detectors (SBD) or photographically by the tracks they leave in a cloud chamber. The SBD has a 300 μm copper window which is "light tight" to soft X-Rays but still "transparent" to energetic electrons. Along with a charge-sensitive preamplifier, the SBD produces about 20 mV per electron in the range 1–10 MeV. The preamplifier saturates at around 2.5 V thus limiting the number of detectable electrons to about 125 (or about 18 electrons/mm^2 with the 3 mm aperture on the SBD) before saturation. The electron track detector is a simple diffusion cloud chamber[20] which uses supersaturated methanol vapor in 1

ATM of air to form visible tracks as electrons ionize the air along their path. The lead-shielded chamber has a 6 μm thick Mylar window over a 3 mm entrance hole located about 5 cm from the vacuum window. The tracks are recorded with a frame-grabbing CCD camera. A uniform, 260 G magnetic field can be applied to the active region of the cloud chamber from coils located outside the lead shielding. The cloud chamber has a much wider dynamic range than the SBD. At low electron fluxes, one can count individual electron tracks while at high fluxes, the brightness of the cloud chamber image can be calibrated (with the 2 MeV linac beam) and shown to be roughly proportional to the flux of electrons, at least up to about 400 electrons/mm^2.

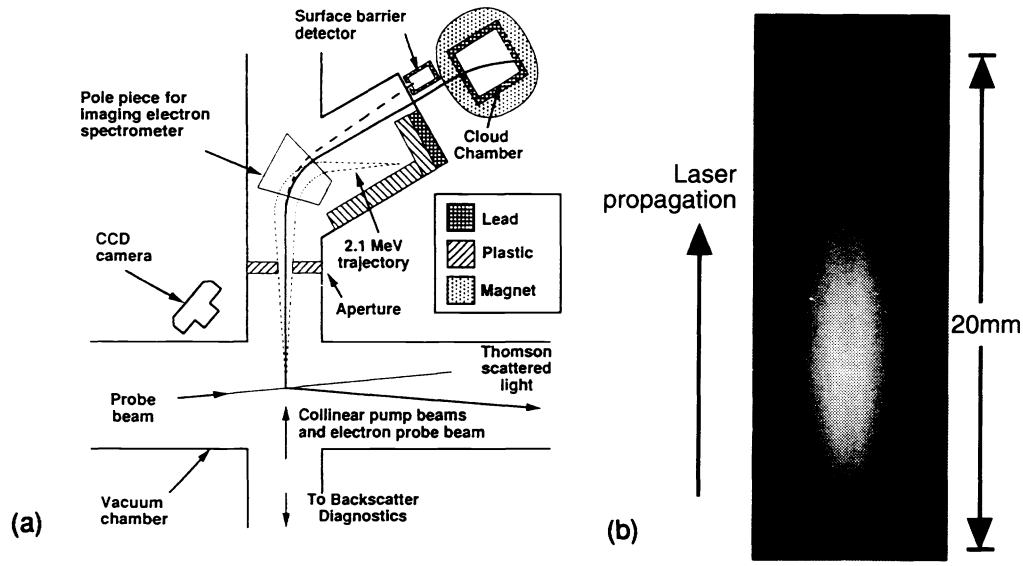

Figure 3: (a) Detailed view of the experimental setup. (b) Time-integrated image of the visible light emitted by the plasma.

3.4. Optical diagnostics

The plasma wave is probed with optical diagnostics as well as with an electron beam. These scattered-light diagnostics, Thomson scattering and CO_2 backscatter, do not probe the beatwave directly, but rather its mode-coupled daughter wave[21] at around $\pm 2\mathbf{k}_1$ due to the presence of an ion acoustic wave at $2\mathbf{k}_1$ from stimulated Brillouin scattering ($\mathbf{k}_1$ is the wavevector for the stronger 10.591 μm pump). In Thomson scattering, a frequency-doubled YAG probe beam of 5 nsec duration is focused to a point within the 10 mm core of the plasma mention earlier. The geometry has been chosen to k-match to waves with $\mathbf{k} = \pm(2.0 \pm 0.5)\,\mathbf{k}_1$. Thus, in addition to mode coupled waves, the diagnostic will pick up scattered light from stimulated Brillouin[22] and Compton[23] driven density fluctuations. The scattered light is sent to a spectrograph/streak camera combination with 0.2 Å and 6 psec resolution. For backscatter, the entire f/11 cone of backscattered light is sampled with a beamsplitter and sent to a spectrograph where the time-integrated spectrum is captured on frame-grabbed pyroelectric camera.

4. EXPERIMENTAL RESULTS

4.1. Plasma emission

The time integrated emission from the plasma is captured with a frame grabber on every data shot to obtain a record of the dimensions, brightness, and location of the plasma. One such image is shown in Fig. 3(b). We see light emission occurring over more than 2 cm around best focus which is consistent with our expectations from Eqs. 1 and 2. Moreover, we see a uniform core of plasma which is approximately 1 cm in

length. Note that the laser intensity varies less than 30% over this core region. Also, the cigar-shaped emission is axially symmetric which suggests that refraction of the laser beam by the plasma is negligible. Indeed, previous studies[17] have shown that the plasma is fully ionized resulting in plasma densities approximately equal to the neutral atomic densities up until the point where refraction begins to be important which occurs for fill pressures beyond about 200 mT and that the plasma temperature is around 75 eV[24]. For our fill pressures, any deviation of the plasma density from the atomic density corresponding to the fill pressure is likely due to hydrodynamic expansion of the plasma during the few hundred psec laser pulse.

4.2. Noise levels and null tests

One of the difficulties of measuring ionizing radiation and electrons in particular is that the commonly employed detectors are sensitive to a variety of radiation sources. For example, surface barrier detectors and scintillator/PMT combinations will produce signals when placed in either an electron environment or an x-ray environment. If one desires to view electrons on these detectors then the x-ray shielding cannot be thicker than the electron range in the shielding material so that shielding against x-rays is inherently limited. Thus in practice there is always some x-ray noise level one must live with. Typical noise levels on our two electron diagnostics are shown in Fig. 4. A histogram of the noise level on the SBD for 80 shots of the linac is shown

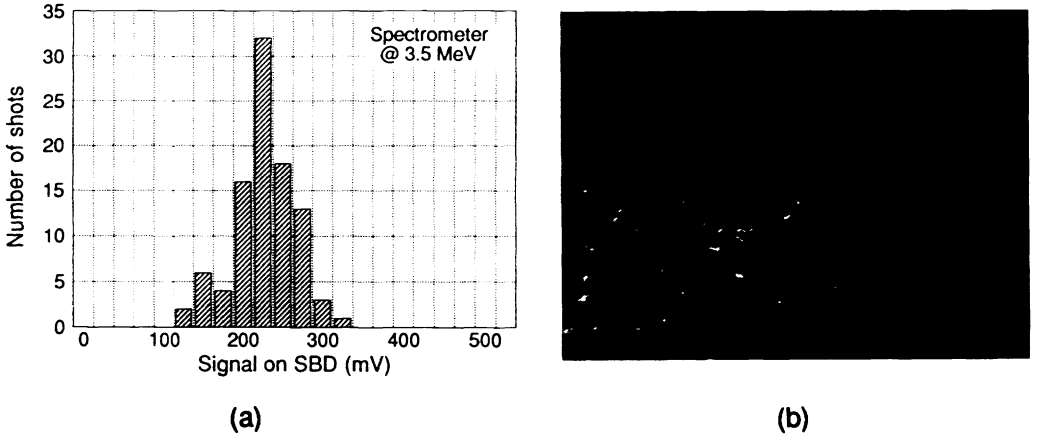

Figure 4: Typical x-ray noise on the surface barrier detector (a) and in the cloud chamber (b).

in Fig. 4(a). Here, the electron spectrometer was set for about 3.8 MeV so that the injected electrons were dumped on the plastic beam dump. We have determined that most of this x-ray noise is from the dumped beam. This same x-ray noise manifests as short, kinked, and randomly oriented tracks in the cloud chamber, as shown in Fig. 4(b). These tracks are produced by secondary electrons ejected from atoms when an x-ray photon is absorbed in the cloud chamber gases. The tracks are typically a few mm to a few cm in length indicating that the electron energies are typically around 10 to 50 KeV. Unlike the SBD detector, the presence of the x-ray noise does not preclude the positive identification of single accelerated electrons. This is because the accelerated electron tracks should be straight, traversing the entire field of view, and constrained to a certain range of angles due to the geometry of the electron spectrometer and cloud chamber aperture.

A series of null tests were performed under various conditions which could, in principle, produce false signals on our detectors. A false signal would be detected electrons not solely due to beat wave acceleration of the injected electrons. These could include electron acceleration by the laser beam itself (no plasma involvement), acceleration of electrons by a Raman instability in the plasma rather than the beat wave, and

the acceleration of background plasma electrons rather than the injected electrons from the linac. Table 2 summarizes these null tests.

4.3. Accelerated electrons

With the linac on and the laser running on two frequencies and firing into a fill pressure of around 140 mT of H_2 gas, accelerated electrons are observed simultaneously with both the SBD and the cloud chamber on a large fraction of the laser shots. Two examples of the cloud chamber data are shown in Figs. 5(a) and

TABLE 2. Summary of the null tests performed and their implications.

Condition of test	Result of test	Implication
•Laser on: 2-frequency operation •Linac on •No plasma (chamber evacuated)	Only the usual† x-ray noise.	No electron acceleration by laser pulse only.
•Laser on: 2-frequency operation •Linac off •Resonant density plasma	No signal at all.‡	No trapping of background plasma electrons or a Raman generated electron tail distribution.
•Laser on: 1-frequency operation •Linac on •Resonant density plasma	Only the usual† x-ray noise.	Raman forward scattering is not growing to substantial levels.

†Usual x-ray noise shown in Fig. 4 and is roughly 10 electrons worth of signal on the SBD's.
‡No signal means less than one electrons worth of signal in the SBD's.

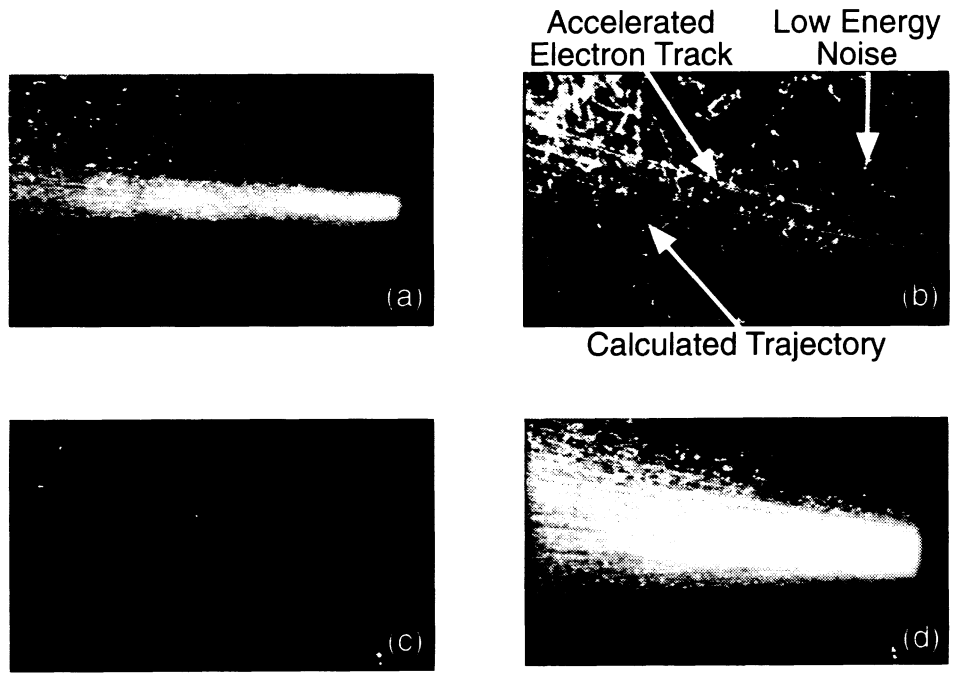

Figure 5: Cloud chamber images. (a) Accelerated electrons at 5.2 MeV with no magnetic field at the cloud chamber. (b) Accelerated electrons at 5.2 MeV with a 260 G magnetic field at the cloud chamber. (c) and (d) Linac electrons at 2.1 MeV at fluxes of 60 and 480 electrons/mm^2, respectively.

(b). Here, the electron spectrometer was set to direct 5.2 ± 0.5 MeV electrons to the cloud chamber and 5.9 MeV electrons to the SBD. In Fig. 5(a) there is no magnetic field and in Fig. 5(b) there is a 260 G magnetic field applied to the cloud chamber to bend the tracks. In Fig. 5(b) we have chosen to display a image with only a few tracks so that we can clearly see the individual electron trajectories and overlay calculated trajectories (the solid white curves in the figure). The good match between the observed and calculated trajectories confirms that these electrons are definitely around 5 MeV in energy, 2.5 times the energy of the injected electrons. The SBD signal corresponding to Fig. 5(b) was 360 mV or about 18 electrons (assuming a SBD sensitivity of about 20 mV/electron) in the same solid angle as seen by the cloud chamber. This agrees closely with the number of actual tracks seen in Fig. 5(b).

The SBD detector was saturated on the shot corresponding to Fig. 5(a) indicating that there were more than 120 electrons through the 3 mm aperture. To get a better idea of how many electrons produced the image in Fig. 5(a), we fired the 2 MeV electrons from the linac itself directly into the cloud chamber (by setting the electron spectrometer to 2 MeV) and varied the output current of the linac to obtain the two images shown in Figs. 5(c) and (d) which bracket the image from accelerated electrons in exposure. The linac output was varied by varying the temperature of the cathode of the thermionic gun. The cloud chamber was then removed and the absolute flux of linac electrons vs. cathode temperature was independently measured using SBD's and a calibrated Faraday cup. From this measurement, we find that the flux of electrons in Figs. 5(c) and (d) are about 60 and 480 electrons/mm^2, respectively. From this, we estimate that the number of electrons in Fig. 5(a) is about 150 electrons/mm^2. From knowledge of the dispersion and vertical imaging properties of the electron spectrometer we estimate that this flux corresponds to a total of about 2×10^4 electrons in the 5.2 ± 0.25 MeV energy bin.

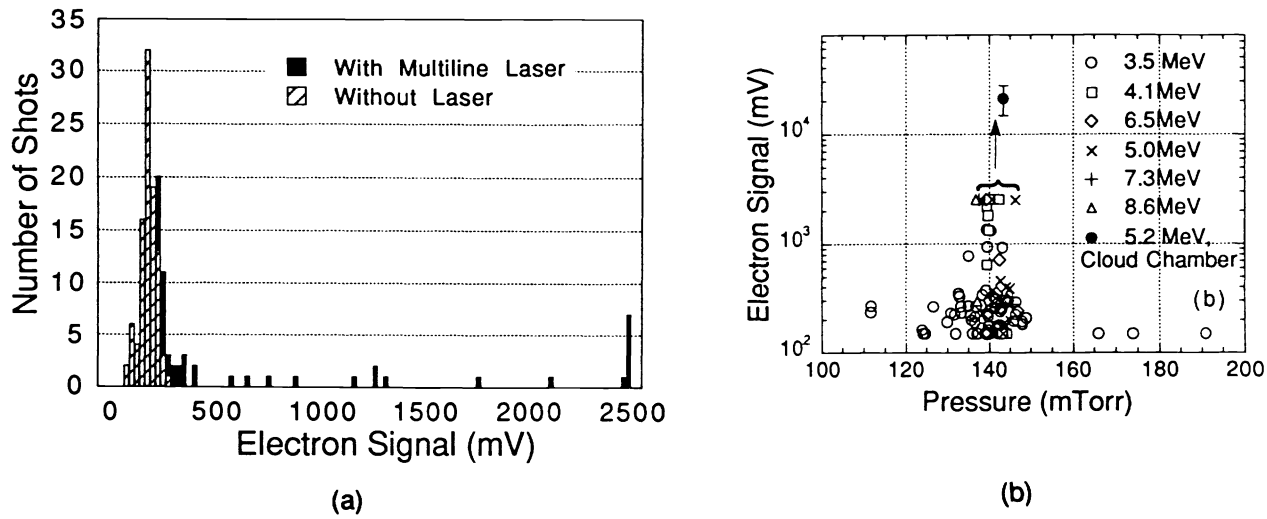

Figure 6: (a) Surface barrier detector signal levels (raw data, in solid bar) and noise histogram (shown in hatched bar). (b) Surface barrier detector signals versus fill pressure of neutral gas. The grouped points with the arrow are saturated on the SBD detector. The highest point is estimated from the cloud chamber images.

The experiment was repeated over a range of fill pressures and with the electron spectrometer set to observe various energies. Figure 6(a) shows a summary of the signals obtained on the SBD's at various acceleration energies. After each shot with a high electron signal, a noise spectrum such as the one shown in

this figure was taken by firing up to 80 linac shots. The noise spectrum in Fig. 6(a) was taken a spectrometer setting of 3.5 MeV. As mention earlier, at higher energy settings the noise level shifts to even lower values. The measured electron signals are clearly many standard deviations larger than the noise, and seven shots saturated the detector. Fig. 6(b) shows the signal levels on the SBD's at various energies vs. the fill pressure. As stated previously, at these laser intensities, fully ionized plasmas are formed up to a plasma density of around 2×10^{16} cm^{-3}. Therefore, we assume that the desired density up to this limit can be obtained by changing the measured gas pressure. From Fig. 1(d), the calculated pressure range over which we would expect a 5% or greater amplitude wave is 126–138 mT with the optimum pressure being 135 mT. Figure 6(b) shows that the signals were essentially in the noise below 135 mT but that there are not enough shots above 148 mT to confirm the exact location of the peak. However, it does appear that the experiment works best with about 5–10 mT higher pressure than the expected optimum. This may be due to some hydrodynamic expansion of the hydrogen plasma during the 70–100 psec growth time of the plasma wave, forcing us to begin with a 4–7% higher initial density. The maximum magnetic field of the electrons spectrometer limited the highest observable energy to 9.1 MeV. Even at this energy, we were still able to saturate the SBD. Thus, many electrons gained *at least* 7 MeV in traversing the roughly 1 cm long plasma wave implying an accelerating gradient of more than 0.7 GeV/m which corresponds to a plasma wave amplitude of at least 8%.

4.4. Estimate of the number of accelerated electrons

In our experiment the injected electron microbunch is not deterministically synchronized to any particular point in the plasma wave with an accuracy (jitter) better than ±100 ps. As a result, the numbers of accelerated electrons can vary greatly from one laser shot to the next. However, by taking a large number of shots one can estimate the maximum number of electrons observed in a particular energy bin and thereby crudely calculate the number of accelerated electrons in a particular energy interval. From the cloud chamber data, we found 2×10^4 electrons at 5.2 MeV within a 0.5 MeV energy bin. The saturated signal at 9.1 MeV indicates that we had at least 125 electrons (2.5 electrons/mm^2 on the SBD) at that energy. Assuming that the accelerated electron spectrum between 5.2 MeV and 9.1 MeV is exponentially decreasing from 2×10^4 to 125, and using the known dispersion of the spectrometer, we estimate that the total number of electrons in this part of the accelerated spectrum is $4 \pm 2 \times 10^4$. Our micropulse contained about 4.25×10^6 electrons in both accelerating and focusing phases of the buckets of the plasma wave. Thus approximately 1% of the available electrons were observed to be accelerated. A better estimate based on the single shot measurement of the complete spectrum of the accelerated electrons is currently under way.

4.5. Correlation with optical diagnostics: Thomson and Raman scatter

The measured electron signals were correlated with optical diagnostics to further confirm that the acceleration observed was associated with the relativistic plasma waves. The time resolved Thomson scattered spectrum is shown in Fig. 7(a). It shows a broad band of scattered frequencies between $0 < (\omega_o - \omega_s) / \Delta\omega < 1.5$ which are due to stimulated Compton scattering (SCS). Here, ω_s and ω_o are the scattered and incident frequencies of the Thomson probe respectively. There is in addition a narrower but much more intense feature at a frequency shift corresponding to $\Delta\omega$. This feature generally shows two temporal bursts. The first has a typical growth time of 50-70 ps and is thought to be due to the mode coupling of the relativistic plasma wave from the still growing ion acoustic wave. As expected, the strongest electron signals were observed on shots when the first burst at $\omega_s = \omega_o - \Delta\omega$ was intense while SCS was still occurring. This is shown in Fig. 7(c). Not all laser shots with a strong burst at $\Delta\omega$ produced electron signals because of the 30–50% probability of the synchronization of the electrons and the plasma wave mentioned earlier. The second peak, which persists after SCS is over, is thought to arise from counter-

propagating optical mixing which excites a slow phase velocity plasma wave. Such a wave cannot accelerate relativistic electrons significantly. The backscatter spectrum, Fig. 7(b), typically shows two distinct peaks on two frequency laser shots. The first peak is shifted from the laser frequency by $\approx 0.8\Delta\omega$, and is present on all two frequency shots. Its location varies 5–10% from shot to shot, and its origin is still being studied. The second peak is shifted from the laser frequency by $\approx \Delta\omega$ (10.9 μm). It appears only on shots in which a plasma beat wave is excited. As with the Thomson scattering diagnostic, the strongest electron signals were observed when the feature at 10.9 μm was relatively intense (see Fig. 7(c)). The correlation of the electron signal with strong scattering signals in the Thomson and the backscatter spectra further supports the notion that the electrons are accelerated by the relativistic plasma wave excited by collinear optical mixing.

As seen in a previous section, the electron energy gain measurements imply that plasma waves of amplitude ε greater than 8% were excited over an approximately 10 mm length in this experiment. Since the maximum energies observed were detection system limited, this average ε is likely to be an underestimate. Local estimates of the relativistic plasma wave amplitude, however, can be made from three features of the Thomson scattered spectra, namely: harmonic components; the mode coupling feature at $\Delta\omega$; and sub-harmonic components. Such estimates[25] indicate that the wave amplitude is much larger than 8%, anywhere from perhaps 15% to greater than 30%. This upper estimate is still around the relativistic detuning limit given earlier. Thus it seems likely that electron energies higher than 9.1 MeV are present in the experiment and efforts are currently underway to measure these higher energies.

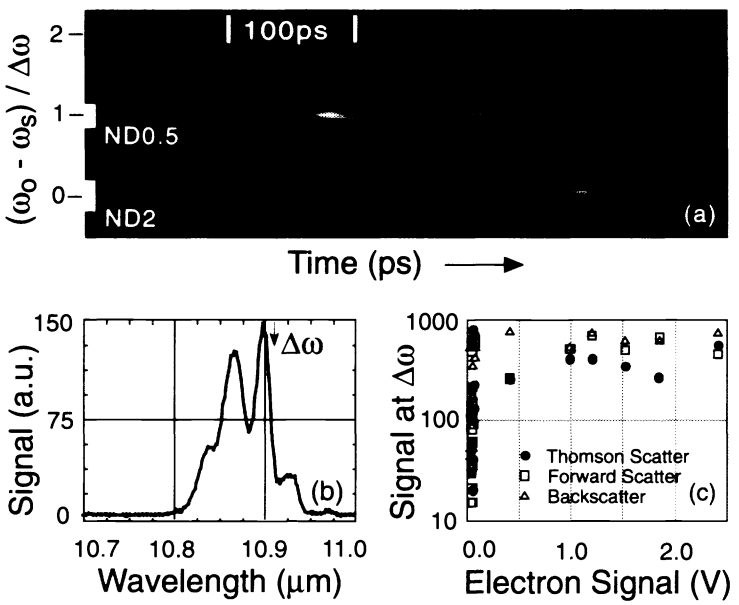

Figure 7: (a) Streak image of Thomson scattered light at $2k_0$. The time scale is indicated on the image. Also, two neutral density filters were place at two frequencies, as indicated. (b) Typical time-integrated backscatter spectrum for two frequency laser operation. (c) Correlation plot of the magnitude of the three optical diagnostics (all Δω–shifted peaks) versus the magnitude of the electron signal on the SBD on the same shots.

4.6. Correlation with forward scatter

Beat wave excitation of a relativistic plasma wave is a four wave process. In addition to the pump waves ω_1 and ω_2 coupling to Stokes sideband at $\omega_1 - \omega_p$ and anti-Stokes sideband at $\omega_2 + \omega_p$ must be

considered. For small plasma wave amplitudes the generation of Stokes and anti-Stokes sidebands can be considered as Bragg scattering of the incident pump waves from the plasma wave. Thus, the observation of the Stokes and anti-Stokes sidebands in the same direction as the pump waves is diagnostically important because not only does it confirm that the relativistic plasmon has been excited but it also can give an independent estimate of the amplitude length product, εL, of this wave. This same quantity is also responsible for the energy gain of electrons since $\varepsilon L \propto E_{accel} L$. In our experiments we monitored a range of frequencies around the Stokes sideband. However, because of the choice of the particular wavelengths and the high laser intensities, we found that rotational Raman scattering in the 100 meters of air (between the laser output window and the vacuum chamber) produced Stokes signals that were comparable to the Stokes radiation generated by the plasma. To try to separate the rotational Raman light from the Stokes light generated from the plasma wave, we blocked a central f/14 cone in the forward scattered light and collected radiation in an annulus out to f/10.5. Since the Stokes radiation should originate in a smaller spot size than the incident radiation, it should therefore be diverging at a larger angle. The resulting Stokes shifted signal had a similar correlation with electrons to that observed with the backscatter and Thomson scatter (Fig. 7(c)), suggesting that the Stokes radiation did originate from the plasma, but more work is needed to conclusively resolve this issue. At any rate, large Stokes signals always accompanied any electron signals indicating at least that we have a two frequency laser pulse where both frequencies are temporally overlapped with one another.

5. CONCLUSIONS

In summary, high-gradient acceleration of externally injected electrons by a relativistic plasma wave excited by a two frequency laser beam has been demonstrated. No accelerated electrons were observed when none were injected or when the laser was operated on a single frequency. However, electrons up to our detection limit of 9.1 MeV were observed when 2.1 MeV electrons were injected in a plasma wave excited (over a narrow range of static gas pressures close to the resonance) by a dual frequency laser beam. The accelerated electron signal was found to be correlated with indirect measurements of the amplitude of the plasma wave using Thomson scattering of an independent probe beam, Raman backscatter of the CO_2 pump beam, and Stokes scatter of the CO_2 pump beam in the forward direction. The energy gain of the electrons suggests plasma wave amplitudes of at least 8% over a 10 mm interaction length. Thomson scattering measurements indicate plasma wave amplitudes up to 15–30%, offering the possibility of measuring even greater energy gains in future experiments.

ACKNOWLEDGMENTS

The authors would like to acknowledge useful discussions with Drs. W. B. Mori and P. Mora, and Professors J. M. Dawson and T. Katsouleas and thank M. T. Shu and D. Gordon for their technical assistance. This work is supported by the U. S. Department of Energy under grant no. DE-FG03-92ER40727.

REFERENCES

1. See, for example, the Special Issue on Plasma-Based High Energy Accelerators, IEEE Trans. Plasma Sc., PS-15, (1987) and C. Joshi, W. B. Mori, T. Katsouleas, J. M. Dawson, J. M. Kindel, and D. W. Forslund, "Ultrahigh gradient particle acceleration by intense laser-driven plasma density waves", Nature 311, 525 (1984).
2. A. T. Tajima and J. M. Dawson, "Laser electron accelerator", Phys. Rev. Lett. 43, 267 (1979).
3. P. Sprangle, E. Esarey, A. Ting, and G. Joyce, "Laser wakefield acceleration and relativistic optical guiding", Appl. Phys. Lett. 53, 2146 (1988).

4. P. Chen, J. M. Dawson, R. W. Huff, and T. Katsouleas, "Acceleration of electrons by the interaction of a bunched electron beam with a plasma", Phys. Rev. Lett. 54, 693 (1985).
5. C. E. Clayton, C. Joshi, C. Darrow, D. Umstadter, "Relativistic plasma wave excitation by collinear optical mixing", Phys. Rev. Lett. 54, 2343 (1985).
6. N. A. Ebrahim, "Lasers, plasmas and particle accelerators – novel particle accelerating techniques for the 21st century", Physics in Canada 45, 178 (1989).
7. Y. Kitagawa, T. Matsumoto, T. Minamihata, K Sawai, K. Matsuo, K. Mima, K Nishihara, H. Azechi, K. A. Tanaka, H. Takabe, and S. Nakai, "Beat-wave excitation of plasma wave and observation of accelerated electrons", Phys. Rev. Lett. 68, 48 (1992).
8. A. E. Dangor, A. K. L. Dymoke-Bradshaw, and A. Dyson, "Observation of relativistic plasma waves generated by the beat-wave with 1 μm lasers", Phys. Scrip. T30, 107 (1990).
9. F. Amironov, M. Laberge, J. R. Marques, F. Moulin, E. Fabre, B. Cros, G. Matthieussent, P. Benkheiri, F. Jacquet, J. Meyer, Ph. Mine, C. Stenz and P. Mora, "Observation of modulational instability in Nd-laser beat-wave experiments", Phys. Rev. Lett. 68, 3710 (1992).
10. C. E. Clayton, K. A. Marsh, A. Dyson, M. Everett, A. Lal, W. P. Leemans, R. Williams, and C. Joshi, "Ultrahigh-gradient acceleration of injected electrons by laser-excited relativistic electron plasma waves", Phys. Rev. Lett. 70, 37 (1993).
11. L. D. Landau and E. M. Lifshitz, Quantum Mechanics (Pergamon, New York 1978).
12. M. Rosenbluth and C. S. Liu, "Excitation of plasma waves by two laser beams", Phys. Rev. Lett. 29, 701, (1972).
13. C. M. Tang, P. Sprangle, and R. N. Sudan, "Dynamics of space-charge waves in the laser beat wave accelerator", Phys. Fluids 28, 1974 (1985).
14. R. L. Williams, C. E. Clayton, C. Joshi, T. Katsouleas and W. B. Mori, "Studies of relativistic wave-particle interactions in plasma-based collective accelerators", Lasers and Particle Beams 8, 427 (1990).
15. K. Marsh, "The design and operation of the electron injector beam line for the plasma beat wave accelerator at UCLA", UCLA PPG-1469, 1992.
16. C. E. Clayton, K. A. Marsh, W. P. Leemans, M. Everett, and C. Joshi, "A terawatt, short-pulse, multiline CO_2 laser facility based on optical free-induction decay" (to be published).
17. W. P. Leemans, C. E. Clayton, W. B. Mori, K. A. Marsh, A. Dyson, and C. Joshi, "Plasma physics aspects of tunnel-ionized gases", Phys. Rev. Lett. 68, 321 (1992) and W. P. Leemans, C. E. Clayton, W. B. Mori, K. A. Marsh, P. K. Kaw, A. Dyson and C. Joshi, "Experiments and simulations of tunnel-ionized plasmas", Phys. Rev. A 46, 1091 (1992).
18. C. E. Clayton and K. A. Marsh, "A 2 MeV, 100 mA electron accelerator for a small laboratory environment", Rev. Sci. Instr., March 1993 (to be published).
19. H. A. Enge, "Deflecting magnets", in Focusing of Charged Particles, edited by A. Septier (Academic, New York 1977), Chap. 4.2.
20. A. Langsdorf, Jr., "A continuously sensitive diffusion cloud chamber", Rev. Sci. Inst. 10, 91 (1939).
21. C. Darrow, D. Umstadter, T. Katsouleas, W. B. Mori, C. E. Clayton, and C. Joshi, "Saturation of beat-excited plasma waves by electrostatic mode coupling", Phys. Rev. Lett. 56, 2629 (1985).
22. C. E. Clayton, C. Joshi, and F. F. Chen, "Ion trapping saturation of the Brillouin instability", Phys. Rev Lett. 51, 1656 (1983).
23. W. P. Leemans, C. E. Clayton, K. A. Marsh, and C. Joshi, "Stimulated Compton scattering from preformed underdense plasmas", Phys. Rev Lett. 67, 1434 (1991).
24. W. P. Leemans, "Topics in high intensity laser plasma interaction", Ph.D. Thesis, UCLA, 1992.
25. C. Joshi, C. E. Clayton, K. A. Marsh, A. Dyson, M. Everett, A. Lal, W. P. Leemans, R. Williams, T. Katsouleas, and W. B. Mori, "Acceleration of injected electrons by the plasma beat wave accelerator", in AIP Proceedings of Workshop on Advanced Accelerator Concepts, Port Jefferson, Ed. J. Wurtele, to be published (1992).